Arch. Metall. Mater. **69** (2024), 3, 1107-1113

DOI: https://doi.org/10.24425/amm.2024.150931

N. NURLINA[1,2], M.N. ALIEF[1], Z. RAHMAWATI[1], S.D. NURHERDIANA[3], T.E. SUSANTO[4], H. FANSURI[1*]

COMPRESSIVE STRENGTH AND WATER FLUX PERFORMANCE OF TYPE C AND TYPE F FLY ASH-BASED GEOPOLYMER MEMBRANE

This study explains the influence of fly ash type C and type F on the properties of membrane geopolymer. The geopolymer paste was synthesized through a mix of fly ash (FA) and an alkaline activator (AA) (2:1 mass ratio of FA:AA). The alkali activator was prepared from sodium silicate and 12 M sodium hydroxide solution in a mass ratio of 1.6. Hydrogen peroxide 3 wt.% was applied as the pore-forming agent, and 4 wt.% glass fiber was employed for reinforcement. The properties of the geopolymer were investigated via Fourier-transform infrared, X-ray diffraction, and scanning electron microscopy. The compressive strength confirmed the higher performance of the type C fly ash-based geopolymer membrane (CFAGM) over the type F fly ash-based geopolymer membrane (FFAGM). On the other hand, FFAGM exhibited an enhanced water permeation flux owing to the larger pore diameter. These results affirmed the excellent performance compared to the previous study.

Keywords: Fly ash; geopolymer membrane; glass fiber; hydrogen peroxide; clean water

1. Introduction

Clean water, as the prevailing demand, is one of the most important targets of the 2030 Sustainable Development Goals (SDGs). The wastewater treatment particularly supports the achievement of SDGs No. 11 and 17, covering goals related to water, health, prosperity, energy, and the environment [1]. In the quest to provide clean water, many technologies have been studied to treat wastewater, including coagulation/flocculation, adsorption, advanced oxidation, and electrochemistry. Among those methods, membrane technology performs superior practicality, high selectivity, and excellent reusability [2]. Additionally, geopolymer exhibits a high efficacy in the removal of pollutants in wastewater, providing increased energy efficiency.

According to the material, membrane is classified into polymer and ceramic. Apart from high filtrating performance, polymer membrane is prone to fouling and impractical at high temperatures and pressure [3]. The ceramic membrane has excellent fouling resistance and is applicable in many various conditions [4]. However, the ceramic membrane is associated with high prices and complicated synthesis procedures that require high temperatures (above 500°C) [5]. From the drawbacks mentioned above, a geopolymer membrane emerges to resolve the fouling issue with a feasible preparation at low temperatures [6].

Geopolymer membrane has sufficient compressive strength within the range of 18.5-62 MPa [7,8] and pore diameter at the nano to micrometer scale [9,10] permitting it to be applied as a bioreactor. Previous studies reported the high achievement of geopolymer membranes with high permeation flux [11] and remarkable selectivity. Notably, the geopolymer membrane is a promising alternative for wastewater filtration. In addition, geopolymer membranes decrease the energy consumption and lower production costs are more energy and cost-saving than conventional ceramic membranes [6]. However, several improvements in membrane characteristics are unavoidably necessary, especially the higher porosity and compressive strength.

The disadvantages displayed by geopolymer are the low bending strength and crack resistance [12], making it unfeasible to be applied as thin as a polymer membrane since this material is brittle. To ensure the feed can pass through without any hinder in certain thickness, the porosity improvement is an utmost inevitability. The porosity of the geopolymer membrane can be

[1] INSTITUT TEKNOLOGI SEPULUH NOPEMBER, FACULTY OF SCIENCE AND DATA ANALYTICS, DEPARTMENT OF CHEMISTRY, SURABAYA 60111, INDONESIA
[2] UNIVERSITAS TANJUNGPURA, FACULTY OF MATHEMATICS AND NATURAL SCIENCE, DEPARTMENT OF CHEMISTRY, PONTIANAK 70124, INDONESIA
[3] UNIVERSITAS PEMBANGUNAN NASIONAL "VETERAN" JAWA TIMUR, FACULTY OF TECHNOLOGY, DEPARTMENT OF CHEMICAL ENGINEERING, SURABAYA 60294, INDONESIA
[4] DEPARTMENT RESEARCH AND DEVELOPMENT PT SEMEN INDONESIA, JAWA TIMUR, INDONESIA

* Corresponding author: h.fansuri@its.ac.id

modified by the addition of pore-forming agents. Sanguanpak et al. [13] applied Al powder to synthesize a metakaolin-based porous geopolymer membrane. Deng et al. [14] utilized hydrogen peroxide (H_2O_2) to synthesize the rich pore structure of the geopolymer membrane. During the hardening process, hydrogen peroxide easily decomposes in an alkaline environment [15] and releases oxygen bubbles leading to the formation of micro and millimeter-sized pores [16]. The effectiveness of H_2O_2 as a pore-forming agent was conveyed by the uniform and well-distributed open pores, as mentioned in other studies [17,18].

The compressive strength of geopolymer membrane depends on the source of silica-alumina materials. Geopolymer membranes can be prepared from widely available materials such as fly ash [19], metakaolin [20], red mud [21], and rice husk ash [22]. Amidst these aluminosilicate materials, fly ash, as generated from the power plant, constitutes the most economically profitable precursor [23,24]. Therefore, the utilization of fly ash as a geopolymer membrane precursor addresses the waste disposal issues [25]. Fly ash is classified into two categories based on the Calcium (Ca) content: Type C and type F. Type C fly ash (CFA) has high Ca while type F has low Ca content [26].

Previous studies have produced fly ash-based geopolymer membranes with compressive strengths of 18.5 MPa. However, despite its 5 mm thickness, this membrane produced a very low water flux (29 $L.m^{-2}.h^{-1}$) [7]. Other research has produced fly ash-based geopolymer membranes utilizing H_2O_2 and starch $(C_6H_{10}O_5)_n$ as pore-forming agents. The resulting membranes have compressive strength of 13.05 MPa and 14.90 MPa, respectively [27]. In addition, Shao et al. [28] synthesized an analcime/geopolymer composite membrane derived from fly ash for organic pollutant filtration with high permeation flux (340-440 $L \cdot m^{-2} \cdot h^{-1}$).

This study investigates the preparation of porous geopolymer membranes from type C and F fly ash with H_2O_2 as a pore-forming agent. Several techniques were adopted to confirm the properties of geopolymer membranes, including mineral composition, functional group, and morphology. The performance of the membrane was defined by the porosity, mechanical strength, and water permeation flux.

2. Experimental

2.1. Materials

The fly ash type C was obtained from the power plan of PT IPMOMI, Probolinggo, while type F was collected from Tanjung Awar-Awar Tuban, East Java, Indonesia. The chemical composition of fly ash was investigated by X-Ray Fluorescence (XRF) analysis, as mentioned in TABLE 1. Pro-analysis (p.a) grade of sodium hydroxide (NaOH) and hydrogen peroxide (H_2O_2) 30% were purchased from Merck. Sodium silicate (Na_2SiO_3) (SiO_2 30.62% and Na_2O 9.42%) was attained locally from PT Brataco.

2.2. Methods

2.2.1. Geopolymer and membrane geopolymer preparation

Prior to the geopolymer preparation, fly ash was sieved at 100 mesh and heated up to 105°C for 24 h. Afterward, 4 wt.% of glass fiber was mixed with this dried fly ash referred to in the previous study by Bai et al. [29]. Separately, the alkaline activator was prepared by the addition of sodium silicate (Na_2SiO_3) into 12 M sodium hydroxide (NaOH) solution at a mass ratio of 1.6:1.

The geopolymer was synthesized by mixing the fly ash (FA)-glass fiber and alkali activator (AA) (2:1 mass ratio of FA:AA) using a hand mixer for 4 minutes. An appropriate amount of 3% H_2O_2 was added, and the stirring was resumed for 2 minutes. The geopolymer paste was cast into a disk shape membrane mold with a 5 mm diameter and 6 mm thickness. For the purpose of compressive strength analysis, the paste was also shaped into a cubic with the dimension of 24 mm×24 mm×24 mm. The geopolymer membrane was attained after the curing process at 55°C for 24 h, followed by the same procedure at room temperature for 2 h. According to the type of fly ash used, the membrane was denoted as type C fly ash geopolymer membrane (CFAGM) and type F fly ash geopolymer membrane (FFAGM).

2.2.2. Characterizations

A Vicat needle technique was applied to study the setting time of the geopolymer. A Vicat needle was periodically inserted into the geopolymer paste in a cylindric mold (20 mm diameter and 60 mm height). The setting time was determined by the total time required for the paste to harden so that the needle could not pass through the geopolymer. Compressive strength was investigated by the universal testing machine using the cube-shaped geopolymer.

Mineral phase analysis of geopolymer was carried out by an Xpert PANalytical X-ray diffractometer using CuKα radiation (λ = 1,5406 Å) at 5-65◦ 2θ with 0.01° step size. An 8400S Shimadzu Fourier Transform Infra-Red (FTIR) was employed to study the functional group of fly ash and geopolymer. The spectra were collected at the wavelength range of 4,000-400 cm^{-1}, where the sample was prepared in a KBr pellet. The morphologies of the samples were observed over scanning electron microscopy (Hitachi Flexsem 1000; coating ion sputtering coxem SPT-20 machine) at an accelerating voltage of 12 kV. The pore diameter was calculated by Image J software.

2.2.3. Water permeability test of geopolymer membrane

A water permeability test was carried out in a dead-end filtration system. In a typical experiment, the geopolymer membrane was placed at the bottom of the reactor, and about 100 ml of water was poured into the filtration chamber. The reactor was

pressurized at 2 bar using an air compressor. The filtration was conducted for 100 minutes, and the filtrate was collected every 20 minutes. The water permeation flux was determined by the following formula:

$$F = \frac{V}{A \times t \times P} \quad (1)$$

where F represents water permeation flux ($L \cdot m^{-2} \cdot h^{-1} \cdot bar^{-1}$), V is the permeate volume (L), A is the surface area of the membrane (m^2), t is the time of filtration (h), and P is pressure (bar).

3. Results and Discussions

3.1. Geopolymer characterizations

The chemical composition of fly ash was analyzed by the XRF technique, as tabulated in TABLE 1. The result was considered in the determination of Si/Al, which was used for the formulation of geopolymer synthesis. It was also confirmed that the CaO content of type C fly ash (CFA) was 3.5 higher than that of type F (FFA). TABLE 2 represents the comparison of CaO content in fly ash for both types. This result was considered for the following study described in the subsequent subchapters.

TABLE 1

Chemical composition of type C and type F fly ash

Chemical Composition	Na_2O	SiO_2	Al_2O_3	CaO	Fe_2O_3	TiO_2	LOI
CFA	2.28	29.67	13.89	21.91	15.48	0.74	3.15
FFA	1.5	46.3	26.4	6.17	11.47	1.93	1.17

TABLE 2

Comparison of results CFAGM and FFAGM properties

Properties	CFAGM	FFAGM
CaO content in raw material (%)	21.91	6.17
Setting time (minutes)	23	225
Pore diameter (mm)	188.95	209.43
Compressive strength (28 days) (MPa)	22.6±3.5	19.7±5.3
Water permeation flux ($L.m^{-2}.h^{-1}.bar^{-1}$)	48.917	356.943

Fig. 1 depicts the diffractograms of fly ash and geopolymer membrane. CFA and FFA generally exhibited two main features: high crystalline and amorphous phases. Quartz (Q) and mullite (M) were the major crystalline phase observed in both CFA and FFA. Hematite (H) and calcite (C) were presented only in CFA, while corundum (Cor) was present in FFA. The amorphous phase was assigned in the form of a hump at 2θ = 20-35°, which is beneficial for geopolymer synthesis [26]. Based on Fig. 1, FFA has a higher intensity of crystal phase than CFA. According to Luhar et al. [30], type F fly ashes that contain low calcium have a higher presence of more crystalline, chemically inert phases.

In terms of CFAGM and FFAGM diffractograms, several differences appeared in some features. A higher intensity of quartz in both membranes represented the additional glass fiber during the preparation. The mullite and quartz intensities slightly decreased that indicating the low dissolution of Si and Al into the alkali solution. The amorphous hump shift from 2θ of 20-35° to 25-40° confirmed the presence of geopolymer with amorphous characteristics [31].

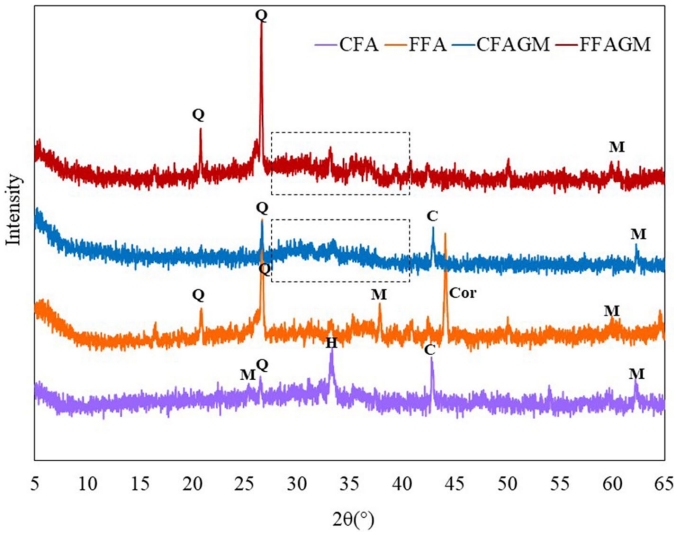

Fig. 1. Diffractogram of CFA, FFA, CFAGM and FFAGM

The functional group of fly ash and geopolymer was analyzed by FTIR, as illustrated in Fig. 2. The O-H stretching mode and bending H-O-H of water molecules were represented by peaks at 3400 and 1650 cm^{-1}, respectively. These peaks were associated with the presence of water adsorbed on the surface. The sharp feature at 900-990 cm^{-1} implied the vibration of Si-O-T (T = tetrahedral Si or Al). This peak shifted to the lower wavenumber for CFAGM and FFAGM samples due to the dissolution of Si and Al during the geopolymerization process [32]. Additionally, the band at approximately 1400 cm^{-1} was attributed to the asymmetric stretching of the O-C-O, inferring the reaction between extra Na^+ or K^+ and atmospheric CO_2 [33].

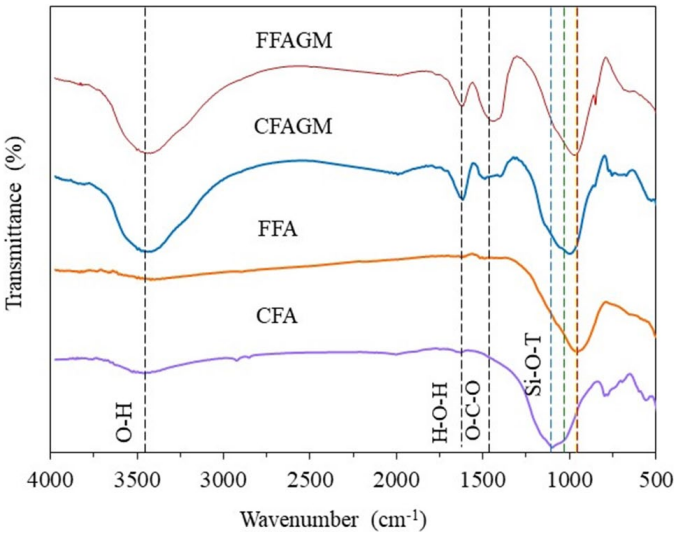

Fig. 2. FTIR spectra of CFA, FFA, CFAGM and FFAGM

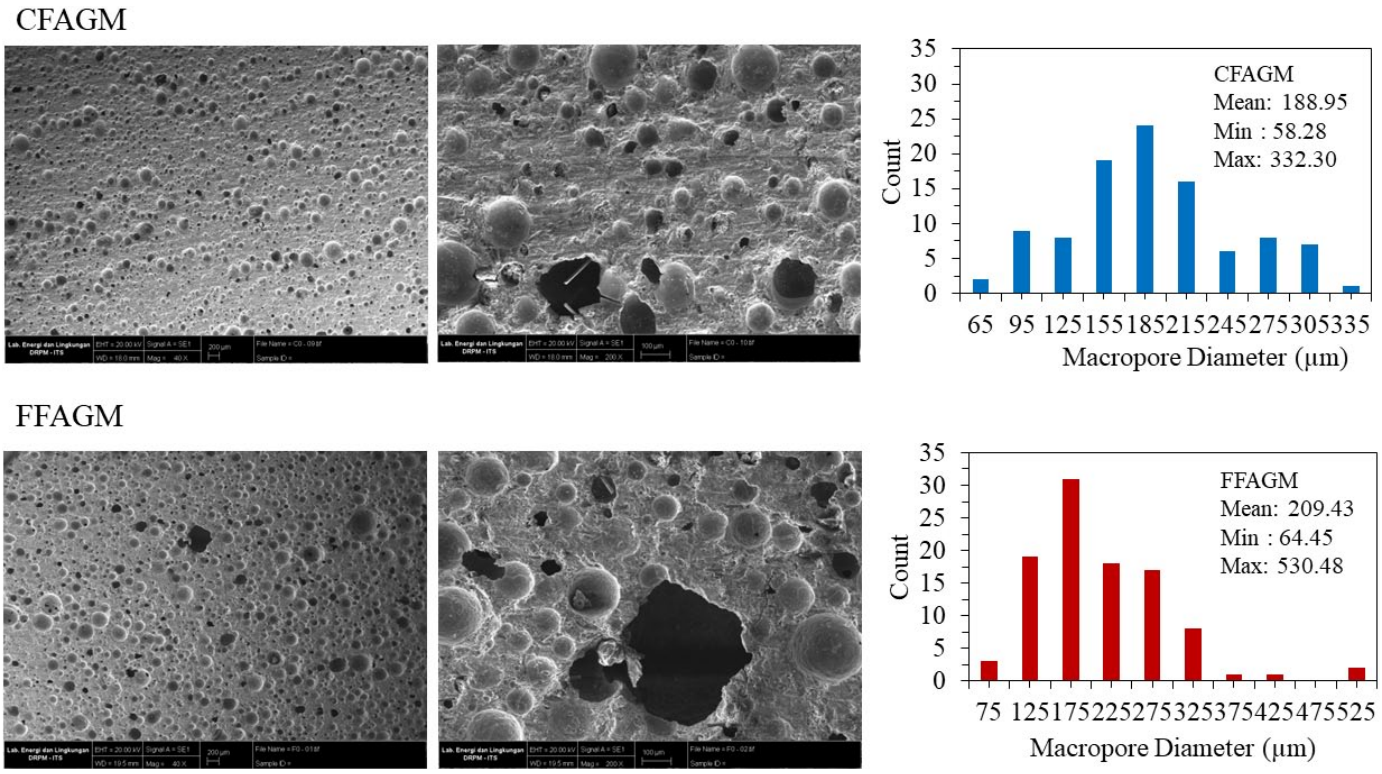

Fig. 3. Cross section and macropore diameter distribution of CFAGM and FFAGM

The morphology of geopolymer membranes is shown in Fig. 3. FFAGM possessed much larger pores compared to CFAGM, with an average pore diameter of 209.43 mm and 188.95 mm, respectively. It is worth noting that the CaO content in the precursor plays a significant role in the decomposition of H_2O_2 during pore formation.

3.2. Setting time and compressive strength of Geopolymer

The setting time of geopolymer was defined by the time required for geopolymer paste to harden. CFAGM sample hardened ten folds faster than FFAGM, as conveyed by the setting time in Fig. 4. The high content of CaO in CFA is responsible for the rapid setting time on CFAGM since the Al^{3+} and Si^{4+} ions formed during fly ash hydrolyze in an alkaline solution, reacted with Ca^{2+} to form calcium silicate hydrate gel (C-S-H), calcium aluminate hydrate gel (C-A-H), or calcium aluminium silicate gel (C-A-S-H), (C = CaO, S = SiO_2, A = Al_2O_3, H = H_2O) [34]. The Ca^{2+} ion enhanced the formation as well as the agglomeration of nuclei in C-A-S-H gel and C-S-H gel [35]. According to Jaya et al. [36], the rapid formation of amorphous C-A-S-H gel and C-S-H gel released high heat of hydration, leading to a shorter setting time. Moreover, Ca^{2+} ions facilitated the polymerization reaction between the silicates and aluminates to produce more N-A-S-H gels.

The hardening time of the geopolymer membrane paste influenced the pore formation by the pore-forming agent. The faster the setting time, the fewer pores generated on the geopolymer membrane, and vice versa (Fig. 3). Small pores were produced during the short setting time where the paste underwent rapid drying. Prolonging the setting time provided an adequate time for H_2O_2 to decompose more, and the bubbles gathered inside the paste to form larger pores [37].

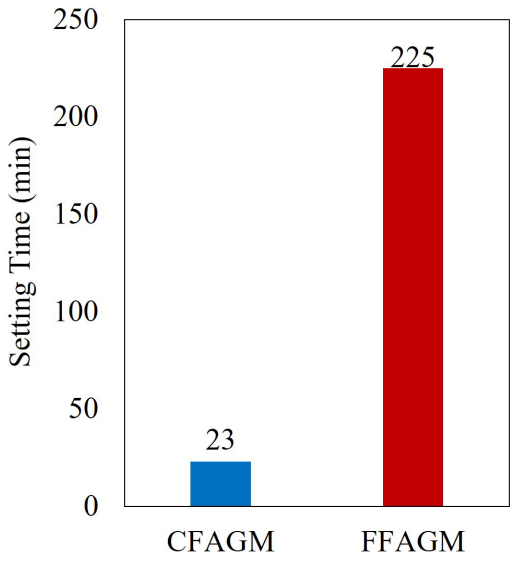

Fig. 4. Setting time of CFAGM and FFAGM

For the purpose of comparison, the aging process was varied into 7 and 28 days before being tested for compressive strength. The results (Fig. 5) inferred that extending the aging time initiated higher compressive strength due to the formation of the longer chains of aluminosilicate oligomers in the form of

polysialate -Si-O-Al- chain or polysialate siloxo -Si-O-Al-O-Si-O- chain or polysialate disiloxo -Si-O-Al-O-Si-O-Si-O chain [38]. Hence, CFAGM 28 days exhibited higher compressive strength (22.6±3.5 MPa) than FFAGM (19.7±5.3 MPa). Beyond 28 days, the aging process generated futile results on geopolymer compressive strength [39]. The compressive strength of CFAGM and FFAGM synthesis in this study was higher compared to the previously reported studies [7,27,40].

The results on the influence of using type C and type F fly ash on the compressive strength of geopolymers are shown in Fig. 5. The compressive strength was related to the CaO content in fly ash precursors. According to Singh et al. [24], fly ash's calcium content contributes significantly to the strength development of geopolymer. In Fig. 5, the compressive strength results of type C fly ash, which contains higher calcium oxide amounts, are higher than type F fly ash with lower calcium oxide amounts. This result is in agreement with the results obtained by Sumer et al. [41]. In the early geopolymerization, the dissolute calcium ions (Ca^{2+}) participate in the formation of 3D network N-A-S-H gels. Calcium ions accelerate the geopolymerization of pastes, contributing to stiffness development and compressive strength enhancement [42].

The high CaO content will accelerate the hardening process, resulting in a denser microstructure and high mechanical strength. On the other hand, lower CaO prolonged the setting process allowing the formation of the larger pore to proceed, leading to lower compressive strength. Based on Fig. 3, FFAGM possessed much larger pores compared to CFAGM. These results support the fact in Fig. 5 that the compressive strength of FFAGM is lower than FFAGM. According to a previous study, the foam released by H_2O_2 as a pore-forming agent was unstable, and large pores often appeared in the final porous geopolymer [15]. The presence of H_2O_2 increases average cell pore size, pore volume fraction, and porosity but reduces the relative density and compressive strength [43,44].

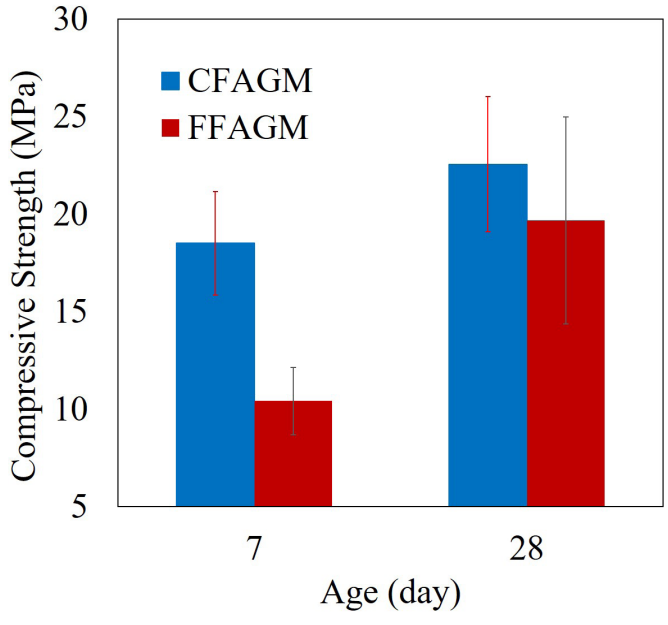

Fig. 5. Compressive strength of CFAGM and FFAGM

3.3. Flux performance of Type C and F fly ash-based geopolymer membrane

The performance of the geopolymer membrane was tested on water permeation flux, as illustrated in Fig. 6. In general, the water permeation flux declined as a function of filtration time. In terms of FFAGM, the permeation flux constantly dropped from 356.943 to 238.4713 $L.m^{-2}.h^{-1}.bar^{-1}$ after 80 minutes and slightly decreased afterward. In comparison, the constant decline proceeded up to 60 minutes from 48.917 to 32.866 $L.m^{-2}.h^{-1}.bar^{-1}$ over CFAGM. The water flux value of CFAGM is more excellent than previously developed geopolymer membranes [7,11,37,40,45-47]. Another researcher also observed the value of the flux as a function of time and reported the same phenomenon [48,49]. According to Chen et al. [50], the decrease in permeability is linked to the reduction in pore size, porosity, and poor connection of pores, which can correlate with the continuance of geopolymerization due to which facilitating by water [51]. Furthermore, FFAGM performed higher permeation flux due to the existence of larger pores compared to the CFAGM.

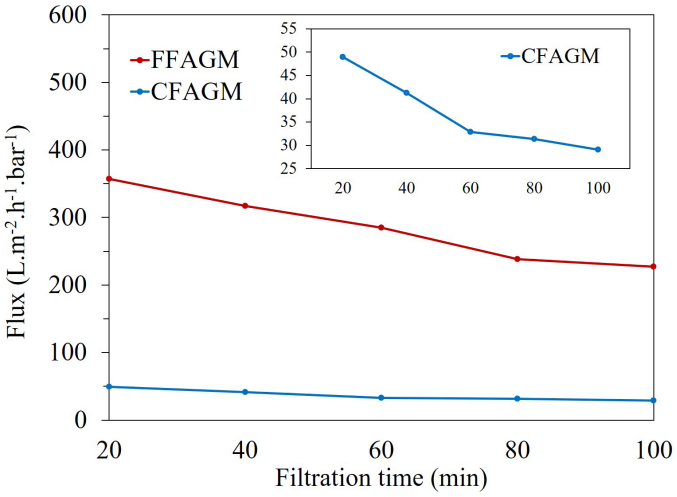

Fig. 6. Water flux performance of FFAGM and CFAGM

Fig. 7 illustrates the role of pores formed by the decomposition of H_2O_2, which decreases the net thickness of the membrane. FFAGM possessed larger pores than CFAGM, resulting in a shorter distance for the feed to pass through the membrane. As a consequence, FFAGM exhibited higher permeation flux. Ge et al. [48] showed that the geopolymer porous structure intensively influenced the water flux. The increased membrane pore size raised the water flux, but the compressive strength was reduced. Xu et al. [11] also reported that larger pores lead to an increase in water flux.

4. Conclusions

Geopolymer membrane was successfully prepared from fly ash types C and F, as confirmed by the diffractogram of XRD and FTIR spectra. The CaO content of fly ash influenced the

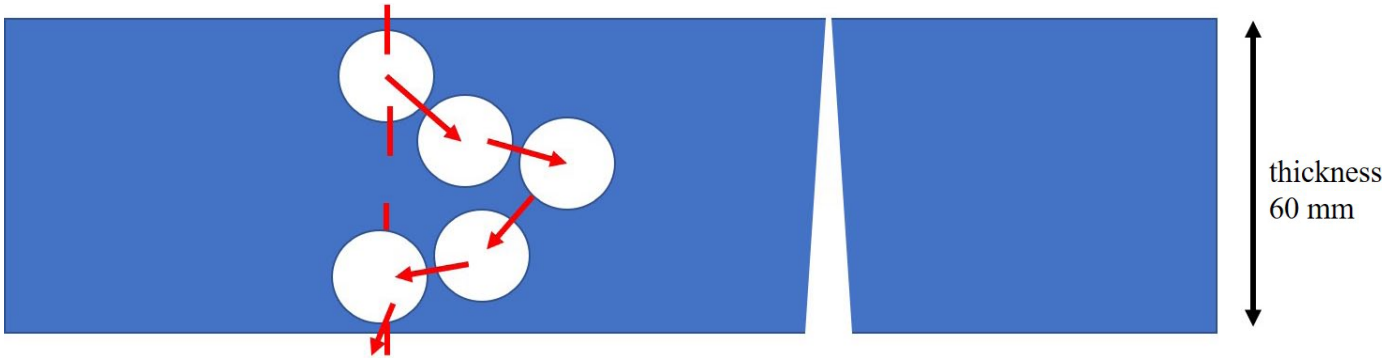

Fig. 7. Illustration of porous in FFAGM

geopolymer membrane's setting time, mechanical strength, and pore size, which affected the performance of the water flux geopolymer membrane. Lower CaO content in type F fly ash hardly fastened the geopolymer hardening time (225 minutes), hereby providing sufficient time for large pore diameter formation (209.43 mm), higher water flux value (356.943 $L.m^{-2}\cdot h^{-1}\cdot bar^{-1}$) but lower compressive strength (19.7±5.3 MPa) than type C fly ash, which required only 23 minutes to set as a hardener geopolymer induced the formation of pores with an average diameter of 188.95 mm, resulted in water flux was 48.917 $L.m^{-2}.h^{-1}.bar^{-1}$ and the compressive strength 22.6±3.5 MPa.

Acknowledgement

The authors gratefully acknowledge the Directorate of Research, Technology, and Community Service of the Indonesian Ministry of Education, Culture, Research, and Technology for the doctoral dissertation research grant under master contract number 084/E5/PG.02.00.PT/2022 on May 10th, 2022, and researcher contract number 1394/PKS/ITS/2022 on May 11th, 2022.

REFERENCES

[1] K. Obaideen, N. Shehata, E.T. Sayed, M.A. Abdelkareem, M.S. Mahmoud, A.G. Olabi, Energy Nexus **7**, 100112 (2022). DOI: https://doi.org/10.1016/j.nexus.2022.100112

[2] R. Kishor, D. Purchase, G.D. Saratale, R.G. Saratale, L.F.R. Ferreira, M. Bilal, R. Chandra, R. N. Bharagava, J. Environ. Chem. Eng. **9**, 2, 105012 (2021). DOI: https://doi.org/10.1016/j.colsurfb.2021.111947

[3] M.N. Zainol Abidin, M. Mahmoud Nasef, T. Matsuura, Polymers (Basel) **14**, (2022). DOI: https://doi.org/10.3390/polym14010197

[4] F. Aouadja, F. Bouzerara, C.M. Guvenc, M.M. Demir, Boletin de La Sociedad Espanola de Ceramica y Vidrio 1 (2021). DOI: https://doi.org/10.1016/j.bsecv.2021.04.002

[5] M. Issaoui, L. Limousy, Comptes Rendus Chimie **22**, 175-187 (2019). DOI: https://doi.org/10.1016/j.crci.2018.09.014

[6] M. Sadiq, A. Naveed, M. Arif, S. Hassan, S. Afridi, M. Asif, S. Sultana, N.U. Amin, M. Younas, M.N. Khan, H. Jiang, S. Gul, Mater. Res. Express **8**, (2021). DOI: https://doi.org/10.1088/2053-1591/ac30e4

[7] A. Naveed, Noor-Ul-Amin, F. Saeed, M. Khraisheh, M. al Bakri, S. Gul, Desalin. Water Treat. **161**, 126-131 (2019). DOI: https://doi.org/10.5004/dwt.2019.24283

[8] A. Naveed, S. Gul, N. Ul Amin, M. Younas, N. Ullah, Desalin. Water Treat. **66**, 203-209 (2017). DOI: https://doi.org/10.5004/dwt.2017.20212

[9] M. Ibrahim, W. Mastura Wan Ibrahim, M. Mustafa Al Bakri Abdullah, A. Syauqi Sauffi, IOP Conf. Ser. Mater. Sci. Eng **864**, (2020). DOI: https://doi.org/10.1088/1757-899X/864/1/012128

[10] J. Huang, Z. Li, J. Zhang, Y. Zhang, Y. Ge, X. Cui, Chem. Eng. J. **397**, 125528 (2020). DOI: https://doi.org/10.1016/j.cej.2020.125528

[11] M. Xue Xu, Y. He, Z. Han Liu, Z. Fa Tong, X. Min Cui, Appl. Clay Sci. **168**, 269-275 (2019). DOI: https://doi.org/10.1016/j.clay.2018.11.024

[12] M. Amran, S. Debbarma, T. Ozbakkaloglu, Constr. Build. Mater. **270**, 121857 (2021). DOI: https://doi.org/10.1016/j.conbuildmat.2020.121857

[13] S. Sanguanpak, W. Shongkittikul, C. Saengam, W. Chiemchaisri, C. Chiemchaisri, Chemosphere **307**, 135760 (2022). DOI: https://doi.org/10.1016/j.chemosphere.2022.135760

[14] X. Deng, Y. He, D. Pan, B. Zhang, X. Cui, Mater. Today Energy **26**, 101016 (2022). DOI: https://doi.org/10.1016/j.mtener.2022.101016

[15] X. Li, C. Bai, Y. Qiao, X. Wang, K. Yang, P. Colombo, J. Clean. Prod. **359**, 132043 (2022). DOI: https://doi.org/10.1016/j.jclepro.2022.132043.

[16] N.B. Singh, Mater. Today Proc. **5**, 15243 (2018). DOI: https://doi.org/10.1016/j.matpr.2018.05.002

[17] G. Masi, W.D.A. Rickard, L. Vickers, M.C. Bignozzi, A. van Riessen, Ceram. Int. **40**, 13891-13902 (2014). DOI: https://doi.org/10.1016/j.ceramint.2014.05.108

[18] G. Roviello, E. Chianese, C. Ferone, L. Ricciotti, V. Roviello, R. Cioff, O. Tarallo, Materials **12**, 4091 (2019). DOI: https://doi.org/10.3390/ma12244091

[19] Z. Chen, X. Wan, Y. Qian, J. Qiao, J. Jia, L. Mo, M. Gao, H. Cui, Y. Liu, F. Min, Constr. Build. Mater. **309**, (2021). DOI: https://doi.org/10.1016/j.conbuildmat.2021.125174

[20] A. Albidah, M. Alghannam, H. Abbas, T. Almusallam, Y. Al-Salloum, J. Mater. Res. Technol. **10**, 84-89 (2021). DOI: https://doi.org/10.1016/j.jmrt.2020.11.104

[21] X. Liang, Y. Ji, SN Appl. Sci. **3**, (2021). DOI: https://doi.org/10.1007/S42452-020-03
[22] S.N. Mahdi, D.V. Babu R.N. Hossiney, M.M.A.B. Abdullah, Case Stud. Constr. Mater. **16**, e00800 (2022). DOI: https://doi.org/10.1016/j.cscm.2021.e00800
[23] Z.W. Paul, N.H.A.S. Lim, M.C. Khun, J. Clean. Prod. **280**, 1 (2021). DOI: https://doi.org/10.1016.j.jclepro.2020.124353
[24] N.B. Singh, Minerals **8**, (2018). DOI: https://doi.org/10.3390/min8070299
[25] A.R.K. Gollakota, V. Volli, C.M. Shu, Sci. Total Environ. **672**, 951-989 (2019). DOI: https://doi.org/10.1016/j.scitotenv.2019.03.337
[26] American Society for Testing and Material, "ASTM C 618-03 Standard Spesification for Coal Fly Ash and Raw or Calcined Natural Pozzolan for Use in Concrete," ASTM International 3 (2003).
[27] A. Naveed, F. Saeed, M. Khraisheh, M. al Bakri, Noor-Ul-Amin, S. Gul, Desalin. Water Treat. **152**, 11-15 (2019). DOI: https://doi.org/10.5004/dwt.2019.23895
[28] N. Shao, S. Tang, S. Li, H. Chen, Z. Zhang, J. Hazard. Mater. **388**, 121736 (2020). DOI: https://doi.org/10.1016/j.jhazmat.2019.121736
[29] C. Bai, P. Colombo, Ceram. Int. **43** (2), 2267-2273 (2017). DOI: https://doi.org/10.1016/j.ceramint.2016.10.205
[30] I. Luhar, S. Luhar, J. Compos. Sci. **6**, 219 (2022). DOI: https://doi.org/10.3390/jcs6080219
[31] C. Ng, U.J. Alengaram, L.S. Wong, K.H. Mo, M.Z. Jumaat, S. Ramesh, Constr. Build. Mater. **186**, 550-576 (2018). DOI: https://doi.org/10.1016/j.conbuildmat.2018.07.075
[32] A.M. Kalinkin, B.I. Gurevich, M.S. Myshenkov, M.V. Chislov, E.V. Kalinkina, I.A. Zvereva, Z. Cherkezova-zheleva, D. Paneva, V. Petkova, Minerals **10**, 1-21 (2020). DOI: https://doi.org/10.3390/min10090827
[33] I.C. Ferreira, R. Galéry, A.B. Henriques, A. Paula De Carvalho Teixeira, C.D. Prates, A.S. Lima, I.R. Souza Filho, J. Mater. Res. Technol. **18**, 4194-4200 (2022). DOI: https://doi.org/10.1016/j.jmrt.2022.03.192
[34] P. Chindaprasirt, P. De Silva, K. Sagoe-Crentsil, S. Hanjitsuwan, J. Mater. Sci. **47**, 4876-4883 (2012). DOI: https://doi.org/10.1007/s10853-012-6353-y
[35] S. Geetha, K. Ramamurthy, Cem. Concr. Compos. **43**, 20-30 (2013). DOI: https://doi.org/10.1016/j.cemconcomp.2013.06.007
[36] N.A. Jaya, L. Yun-Ming, H. Cheng-Yong, M.M.A.B. Abdullah, K. Hussin, Constr. Build. Mater. **247**, 118641 (2020). DOI: https://doi.org/10.1016/j.conbuildmat.2020.118641
[37] M. Xue Xu, Y. He, C. Qun Wang, X. Feng He, X. Qing He, J. Liu, X. Min Cui, Appl. Clay Sci. **115**, 254-259 (2015). DOI: https://doi.org/10.1016/j.clay.2015.03.019
[38] X.Y. Zhuang, L. Chen, S. Komarneni, C.H. Zhou, D.S. Tong, H.M. Yang, W.H. Yu, H. Wang, J. Clean. Prod. **125**, 253 (2016). DOI: https://doi.org/10.1016/j.jclepro.2016.03.019
[39] R.E. Hidayati, F.S. Faradilla, D. Dadang, L. Harmelia, N. Nurlina, D. Prasetyoko, H. Fansuri, Arch. Metall. Mater. **66**, 1115-1121 (2021). DOI: https://doi.org/10.24425/amm.2021.136431
[40] M.R. Abukhadra, M.H. Eid, A.M. El-Sherbeeny, A.E.E. Abd Elgawad, J.J. Shim, J. Contam. Hydrol. **244**, 103923 (2022). DOI: https://doi.org/10.1016/j.jconhyd.2021.103923
[41] M. Sumer, Constr. Build. Mater. **34**, 531-536 (2012). DOI: https://doi.org/10.1016/j.conbuildmat.2012.02.023
[42] X. Zhao, C. Liu, L. Zuo, L. Wang, Q. Zhu, M. Wang, Cem. Concr. Compos. **103**, 279-292 (2019). DOI: https://doi.org/10.1016/j.cemconcomp.2018.11.019
[43] C. Bai, P. Colombo, Ceram. Int. **43**, 2267-2273 (2016). DOI: https://doi.org/10.1016/j.ceramint.2016.10.205
[44] A. Hajimohammadi, T. Ngo, P. Mendis, T. Nguyen, A. Kashani, J.S.J. van Deventer, Mater. Des. **130**, 381-391 (2017). DOI: https://doi.org/10.1016/j.matdes.2017.05.084
[45] Y. Song, Z. Li, J. Zhang, Y. Tang, Y. Ge, X. Cui, ACS Appl. Mater. Interfaces **12**, 12133-12142 (2020). DOI: https://doi.org/10.1021/acsami.0c00440?ref=pdf
[46] L. Chen, K. Zheng, Y. Liu, Constr. Build. Mater. **151**, 63-70 (2017). DOI: https://doi.org/10.1016/j.conbuildmat.2022.127064
[47] S. Subaer, H. Fansuri, A. Haris, M. Misdayanti, I. Ramadhan, T. Wibawa, Y. Putri, H. Ismayanti, A. Setiawan, Membranes (Basel) **12**, (2022). DOI: https://doi.org/10.3390/membranes12111046
[48] Y. Ge, Y. Yuan, K. Wang, Y. He, X. Cui, J. Hazard. Mater. **299**, 711-718 (2015). DOI: https://doi.org/10.1016/j.jhazmat.2015.08.006
[49] N. Shamsuddin, C. Cao, V.M. Starov, D.B. Das, Water Sci. Technol. Water Supply **16**, 481-492 (2016). DOI: https://doi.org/10.2166/ws.2015.158
[50] S. Chen, S. Ruan, Q. Zeng, Y. Liu, M. Zhang, Y. Tian, D. Yan, Constr. Build. Mater. **328**, 127064 (2022). DOI: https://doi.org/10.1016/j.conbuildmat.2022.127064
[51] S. Park, M. Pour-Ghaz, Constr. Build. Mater. **182**, 360-370 (2018). DOI: https://doi.org/10.1016/j.conbuildmat.2018.06.073